Proceedings of the ASME 2024 7th International Conference on
Micro/Nanoscale Heat and Mass Transfer
MNHMT2024
August 5-7, 2024, Nottingham, UK

MNHMT2024-121445

EXPERIMENTAL INSIGHTS INTO THERMAL-HYDRAULIC PERFORMANCE OF A COMPACT PRINTED CIRCUIT HEAT EXCHANGER WITH AIRFOIL FINS USING HIGH-PRESSURE WATER

Weitong Liu [1,2], Haoxing Zhi [1,2], Han Qi [2], Yanchen Fu [1,2,*]

[1] Research Institute of Aero-engine, Beihang University, Beijing 100191, China
[2] Collaborative Innovation Center for Advanced Aero-Engine,
Beihang University, Beijing 100191, China

ABSTRACT

Printed Circuit Heat Exchanger (PCHE) has emerged as a promising candidate for advanced thermal management systems, owing to its high compactness, efficiency, and remarkable reliability under harsh conditions such as high pressure and temperature. The present study constructs an experimental platform with two high-pressure water loops to experimentally investigate the thermal-hydraulic performance of the airfoil-fin PCHE with a hydraulic diameter of 0.87 mm. The heat transfer capacity of the PCHE is beyond 175 kW and the surface-area-to-volume ratio is larger than 1500 m^2/m^3. The experimental data is obtained at the Reynolds number (Re) ranging from 65.4 to 444 and inlet pressure ranging from 1.58 MPa to 2.75 MPa. The friction coefficient correlation is developed within ±10% deviation with the experimental data. The Nu correlation is also proposed, having a maximum deviation of ±20%. The thermal-hydraulic characteristics of high-pressure water in the PCHE are analyzed, indicating that airfoil-fin PCHE exhibits excellent thermal-hydraulic performance. At extremely low Re (Re_h = 199.4 and Re_c = 165.4), the overall heat transfer coefficient can still reach 1370.5 $W/m^2/K$. The present work can contribute to designing and optimizing high-performance PCHE with airfoil fins.

Keywords: Printed circuit heat exchanger; airfoil-fin channel; heat transfer; pressure drop

NOMENCLATURE

A	Heat transfer area [m^2]
A_c	Cross-sectional area [m^2]
c_p	isobaric specific heat capacity [J/kg/K]
d	hydraulic diameter [mm]
f	Friction coefficient
h	Heat transfer coefficient [$W/m^2/K$]
K	Overall heat transfer coefficient [$W/m^2/K$]
L	Distance between core inlet and core outlet [m]
m	Mass flow rate [g/s]
Nu	Nusselt number
Pr	Prandtl number
P	Pressure [MPa]
ΔP	Pressure drop [kPa]
P_{fin}	Perimeter of the fin [m]
Q	Heat transfer rate [kW]
R	The overall thermal resistance of PCHE [K/W]
Re	Reynolds number
S	The side surface area of the element [m^2]
S_{top}	The top surface area of the fin [m^2]
T	Temperature [°C]
ΔT_m	Logarithmic mean temperature difference [°C]
u	Velocity [m/s]
V	The volume of the element [m^3]

Greek symbols

α	Constant
β	Constant
Δ	Difference
δ	Wall thickness [mm]
μ	Dynamic viscosity [μPa·s]
λ	Thermal conductivity [W/m/K]

Subscripts

ave	Average
core	PCHE core
c	Cold fluid
h	Hot fluid
in	Inlet
out	Outlet
cal	Calculated data
exp	Experimental data
w	Wall

Abbreviations

HTC	Heat transfer coefficient
PCHE	Printed circuit heat exchanger
NACA	National Advisory Committee for Aeronautics
SUS	Steel Use Stainless

1. INTRODUCTION

With the rapid development of advanced energy and power systems, there is a growing demand for more compact, efficient, and stable heat transfer technologies. Compared to traditional heat exchangers such as plate-fin, tube-shell, tube-fin types, and so on, the Printed Circuit Heat Exchanger (PCHE), owing to its high compactness, efficiency, and remarkable reliability under harsh conditions such as high pressure and temperature, has emerged as a promising candidate [1]. Consequently, scholars are working towards the successful application of PCHE in fields such as supercritical CO_2 Brayton cycle [2], high-temperature gas-cooled reactors [3], sodium-cooled fast reactors [4], waste heat recovery systems [5], aero engine thermal management systems [6, 7], etc.

The flow passages of PCHE are manufactured by photochemical etching, easily forming microchannels with hydraulic diameters ranging from millimeters to micrometer scales. By stacking together the plates and using diffusion bonding technology, PCHE achieves high strength comparable to its base material, ensuring long-term reliability. Currently, there are four primary configurations of PCHE flow channels: straight, zigzag, S-shape, and airfoil [8]. Among them, PCHE with airfoil fins is considered to have the best comprehensive thermal-hydraulic performance [9], making it a recent research focus. However, research on the heat transfer and pressure drop correlations of PCHE with airfoil fins through experiments is currently quite limited, posing challenges for the precise design and optimization of PCHE with airfoil fins. Wang et al. [10] experimentally investigated the heat transfer performance of a PCHE, using the ternary salt in the airfoil channel and the synthetic oil in the straight channel. Shi et al. [11] developed the heat transfer and friction factor correlations for molten salt and supercritical carbon dioxide in the airfoil channel of PCHE through numerical simulation. Han et al. [12] introduced a novel airfoil fins PCHE with flue gas on the hot side and water on the cold side. The Nusselt number (*Nu*) correlation was proposed for flue gas in the airfoil channel, while the *Nu* correlation of water in the airfoil channel was directly used the Hausen equation [13]. The thermal-hydraulic performance of an asymmetric airfoil-fin PCHE using supercritical carbon dioxide was explored by Chang et al. [14]. It indicated that the forward flow has a better comprehensive performance. Meanwhile, a heat transfer correlation for supercritical CO_2 flowing in the asymmetric airfoil-fin PCHE with different directions was proposed. In the research of Chuang et al. [15], the heat transfer performance and pressure drop of nitrogen in a PCHE with airfoil and straight channels were analyzed. Their results reveal that the Gnielinski correlation has sufficient precision to predicit the *Nu* in the case of PCHE with straight channels.

However, it becomes apparent that the majority of existing research on airfoil-fin PCHE relies heavily on numerical simulations, with limited experimental studies. Furthermore, investigations have primarily focused on working fluids such as supercritical CO_2 and helium. Despite water being one of the most common heat transfer fluids, there is limited research on its flow and heat transfer characteristics within airfoil-fin PCHE. Especially notable is the absence of experimental research focusing on the heat transfer and pressure drop correlations of water within airfoil-fin PCHE, posing challenges for the precise design and optimization of PCHE with airfoil fins.

The present study addresses this gap by experimentally investigating the thermal-hydraulic performance of a PCHE with NACA0025 airfoil fins. A thermodynamic performance test rig was established, comprising a hot water loop and a cold water loop. Experimental studies were conducted to investigate the heat transfer and pressure drop characteristics with variations in water mass flow rates and heat loads. This study focuses on developing *Nu* and friction factor correlations, with high-pressure water serving as the working medium.

2. EXPERIMENTAL SETUP AND DATA REDUCTION

2.1 PCHE test section

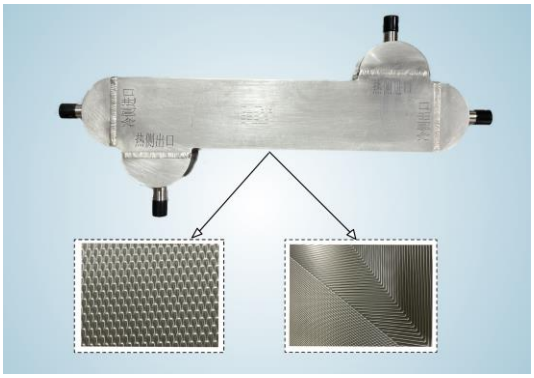

FIGURE 1: DIAGRAM OF THE PCHE TEST SECTION.

In the present work, a PCHE with a hydraulic diameter of 0.87 mm was fabricated using alternately stacked SUS316L plates consisting of 25 plates for the hot side and 26 plates for the cold side. The plates have a length of 601.2 mm, a width of 153 mm, and a height of 1.2 mm. and the PCHE core dimension is 601.2 mm × 153 mm × 86 mm. Moreover, the cold-side and hot-side plates are both equipped with identically sized staggered NACA0025 airfoil fins to form the channels. The number of channels in one plate is 102. The distinction lies in the hot-side plate, which features a small "L-shaped" straight channel region in the inlet and outlet areas for a more rational arrangement of the headers, as illustrated in FIGURE 1. The PCHE adopts a counterflow configuration to achieve better heat transfer performance. The heat transfer capacity of the PCHE is larger than 175 kW and the surface-area-to-volume ratio is larger than 1500 m^2/m^3, positioning it as a robust solution for applications in high-performance thermal management systems.

FIGURE 2 shows the schematic of the airfoil fin arrangement. The chord length (L_c), width (W_f), and height (H) of the airfoil fin are 2.4 mm, 0.6 mm, and 0.8 mm, respectively. The fins are arranged in a staggered arrangement with a

staggered pitch (L_{st}) of 2.4 mm, a longitudinal pitch (L_v) of 4.8 mm, and a transverse pitch (L_s) of 1.2 mm. The key geometrical parameters of the airfoil fin are summarized in Table 1.

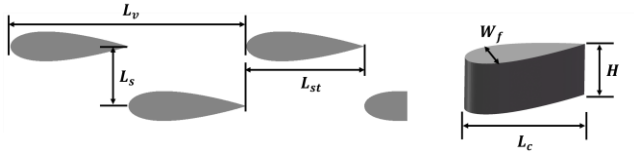

FIGURE 2: SCHEMATIC OF AIRFOIL FIN ARRANGEMENT.

TABLE 1: GEOMETRICAL PARAMETERS OF THE FIN.

Parameters	Value	Parameters	Value
Chord length, L_c	2.4 mm	Staggered pitch, L_{st}	2.4 mm
Width, W_f	0.6 mm	Longitudinal pitch, L_v	4.8 mm
Height, H	0.8 mm	Transverse pitch, L_s	1.2 mm
Perimeter, P_{fin}	5.1 mm	Top surface area, S_{top}	0.98 mm^2

2.2 Experimental system

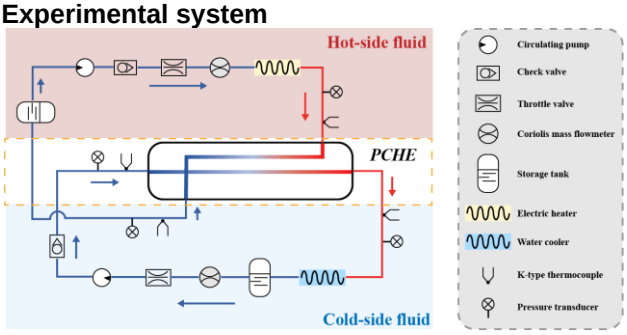

FIGURE 3: SCHEMATIC OF PCHE EXPERIMENTAL SYSTEM.

The thermodynamic performance test rig for the PCHE was established comprising 3 sub-systems: the hot-side fluid loop, the cold-side fluid loop, and the data acquisition system, as presented in FIGURE 3. High-pressure water is utilized as the working fluid on both the hot side and cold side. Along the hot-side fluid loop, room-temperature water is stored in the storage tank and is pre-pressurized to a specified pressure by high-pressure nitrogen. High-pressure water is circulated by a circulating pump, passing through a check valve. It is then regulated and measured separately using a throttle valve and a Coriolis mass flow meter. Subsequently, an electric heater is employed to raise the water to a predefined temperature. After that, the high-temperature water exchanges heat with the cold-side fluid in the PCHE with NACA0025 airfoil fins and flows back to the storage tank. Regarding the circulation of the cold-side fluid, the experimental system is essentially the same as the hot-side fluid loop. The difference lies in the fact that room-temperature water, after being heated inside the PCHE, is cooled back to room temperature through a water cooler before returning to the storage tank. The data acquisition system utilized multiple K-type sheathed thermocouples and ROSEMOUNT pressure transmitters at the inlets and outlets of the PCHE to collect temperature and pressure data. All the tubes and test sections are thermally insulated with thermal insulation material. Given the capabilities of the test rig, the water can reach a maximum temperature of 200°C, a maximum pressure of 4.5 MPa, and a maximum mass flow rate of 630 g/s.

2.3 Data reduction

The current work constructed the PCHE experimental system with two high-pressure water loops to explore the thermal-hydraulic performance of the airfoil-fin PCHE. The processing of experimental data is carried out using the following formulas.

It is difficult to define an appropriate hydraulic diameter (d) for the airfoil-fin channel. The definition in Ref. [16] has been widely accepted as applicable to airfoils with different geometry parameters. The hydraulic diameter (d) can be calculated by Eqs. (1)-(3).

$$d = \frac{4V}{S} \tag{1}$$

$$V = (L_v L_s - S_{top})H \tag{2}$$

$$S = P_{fin}H + 2(L_v - L_c)H + 2(L_v L_s - S_{top}) \tag{3}$$

where V and S are the volume and the side surface area of the element channel, respectively. Since the hot side and the cold side have the same airfoil fin channel, the hydraulic diameters of both the cold side and the hot side are identical.

The Reynolds number (Re) of the fluid on both sides is defined as below. The thermal properties of high-pressure water and their uncertainties are obtained from the CoolProp Library [17].

$$Re = \frac{4m}{\mu\pi d} \tag{4}$$

where μ is the dynamic viscosity of the fluid.

The determination of heat transfer rates to the hot-side water, and cold-side water involves analyzing the measured mass flow rates (m_h, m_c), the temperatures of different working fluids, and the isobaric specific heat capacity (c_p) of the fluids at average temperature ($T_{ave} = (T_{in}+T_{out})/2$), as follows.

$$Q_h = m_h c_{p,h}\left(T_{h,\text{in}} - T_{h,\text{out}}\right) \tag{5}$$

$$Q_c = m_c c_{p,c}\left(T_{c,\text{out}} - T_{c,\text{in}}\right) \tag{6}$$

$$Q_{ave} = \frac{Q_c + Q_h}{2} \tag{7}$$

where subscript h for hot-side water, c for cold-side water, in for inlet, and out for outlet. Q_{ave} is the average heat transfer rate of the PCHE.

The logarithmic mean temperature difference of the PCHE is shown in Eq. (8).

$$\Delta T_m = \frac{\left(T_{h,\text{in}} - T_{c,\text{out}}\right) - \left(T_{h,\text{out}} - T_{c,\text{in}}\right)}{\ln\left(\dfrac{T_{h,\text{in}} - T_{c,\text{out}}}{T_{h,\text{out}} - T_{c,\text{in}}}\right)} \tag{8}$$

The overall heat transfer coefficient is computed by the following equation.

$$K = \frac{Q_{ave}}{\Delta T_m A} \tag{9}$$

K can also be written as:

$$K = \frac{1}{\frac{A}{A_h}h_h + \frac{A\delta}{A_w\lambda_w} + \frac{A}{A_c}h_c} \quad (10)$$

where h_h, h_c is the heat transfer coefficient (HTC) of the hot-side fluid, and cold-side fluid, respectively; A_h, A_w, A_c is the heat transfer area of the hot fluid side, cold fluid side, and wall, respectively; δ represents wall thickness; λ_w is the thermal conductivity of the wall, which is 16.3 W/m/K.

The overall thermal resistance of the PCHE can be calculated by Eq. (11).

$$R = \frac{1}{KA} = \frac{\Delta T_m}{Q_{ave}} = \frac{1}{h_h A_h} + \frac{\delta}{A_w\lambda_w} + \frac{1}{h_c A_c} \quad (11)$$

The Nusselt number and Prandtl number (Pr) are defined as below.

$$Nu = \frac{hd}{\lambda} \quad (12)$$

$$Pr = \frac{\mu c_p}{\lambda} \quad (13)$$

The friction coefficient can be calculated by Eq. (14).

$$f = \Delta P_{core}\frac{d}{L}\frac{1}{(1/2)\rho u^2},\ u = \frac{m}{\rho A_c} \quad (14)$$

where ΔP_{core} is the pressure drop of the PCHE core; u is the fluid velocity; A_c represents the cross-sectional area; L is the distance between the core inlet and core outlet.

2.4 Uncertainty analysis

TABLE 2: RANGE AND UNCERTAINTIES OF DIRECT MEASUREMENTS.

Direct measurement	Range	Uncertainty
Hot side mass flow rate	0-0.5 kg/s	±0.2%
Cold side mass flow rate	0-2 kg/s	±0.2%
Temperature	223.15-1423.15 K	±1.5 K
Absolute pressure	0-10 MPa	±0.04%
Pressure drop	0-100 kPa	±0.04%

The working range and uncertainty of direct measurements are summarized in Table 2. For the uncertainties of indirect measurements, the current study adopts the method described in Ref. [18]. Given measurements with uncertainties δx_1, δx_2, …, δx_n for variables x_1, x_2, …, x_n, the values obtained are used in the computation of the variable (y) based on Eq. (15). If uncertainties in x_1, x_2, …, x_n are independent and random, the uncertainty in y is expressed by Eq. (16). The calculated relative uncertainties of Q_{ave}, K, and Re is 2.14%, 2.31%, and 0.55%, respectively.

$$y = f\left(x_1, x_2, ..., x_n\right) \quad (15)$$

$$\delta y = \sqrt{\left(\frac{\partial y}{\partial x_1}\delta x_1\right)^2 + \left(\frac{\partial y}{\partial x_2}\delta x_2\right)^2 + \cdots + \left(\frac{\partial y}{\partial x_n}\delta x_n\right)^2} \quad (16)$$

3. RESULTS AND DISCUSSION

3.1 Specification of experimental conditions and heat balance

The thermal-hydraulic performance of the airfoil-fin PCHE using high-pressure water was experimentally investigated under various operation conditions. FIGURE 4 depicts the Re, average temperature, and inlet pressure of all experimental data points for both hot-side fluid and cold-side fluid. The max heat load of the test conditions is 37.50 kW. Due to the thermal insulation material wrapping around all the tubes and PCHE, and considering the working medium is water with a high specific heat capacity, heat losses during the experiment have been minimized to the greatest extent possible. The detailed experimental conditions are summarized in Table 3.

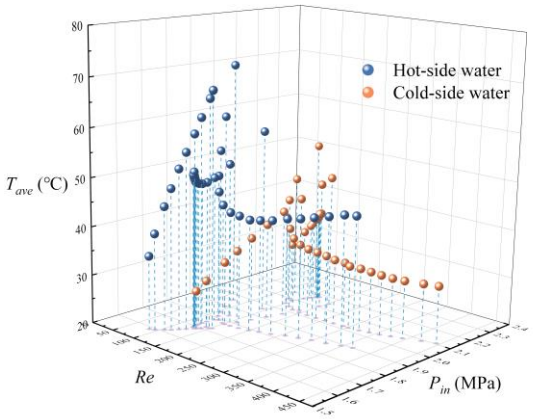

FIGURE 4: REYNOLDS NUMBER, INLET PRESSURE, AND TEMPERATURE OF ALL EXPERIMENTAL DATA POINTS.

TABLE 3: EXPERIMENTAL CONDITIONS.

Parameters	Hot side	Cold side
Mass flow rate	52.8-372.3 g/s	53.5-621.6 g/s
Reynolds number	75.1-365.8	65.5-444.0
Inlet Pressure	1.58-2.75 MPa	1.69-2.73 MPa
Inlet temperature	50.45-120.25℃	19.50-26.50℃

FIGURE 5 illustrates the comparison of heat transfer rates between the hot-side fluid and the cold-side fluid of the experimental data. The observed deviation between the two sides is within ±10%, suggesting that the experimental data obtained in this study is reliable.

To explore the overall heat transfer performance of the PCHE, the overall HTC of all experimental data on the basis of the cold-side heat transfer area (K_c) is calculated by Eq. (9), the results are shown as a function of Re_c and Re_h in FIGURE 6. The maximum K_c is 1370.5 W/m^2/K, occurring when Re_h = 199.4 and Re_c = 165.4. Considering the relatively low Reynolds numbers of the cold and hot side fluids at this point, indicative of laminar flow, the airfoil-fin PCHE exhibits a higher overall heat transfer coefficient and superior heat transfer performance compared to other types of heat exchangers such as shell-and-tube heat exchangers and plate-fin heat exchangers.

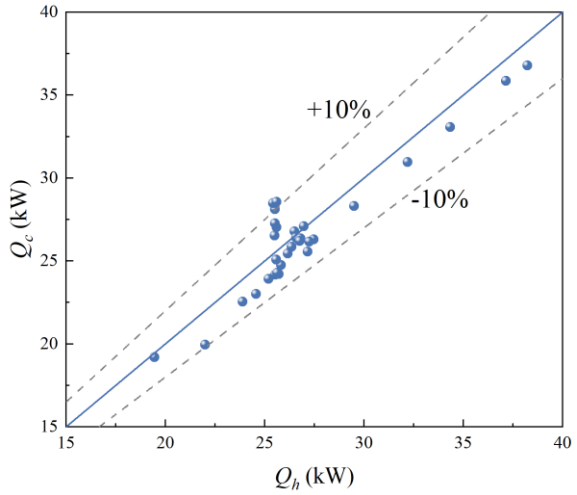

FIGURE 5: COMPARISON OF HEAT TRANSFER RATES BETWEEN HOT-SIDE FLUID AND COLD-SIDE FLUID.

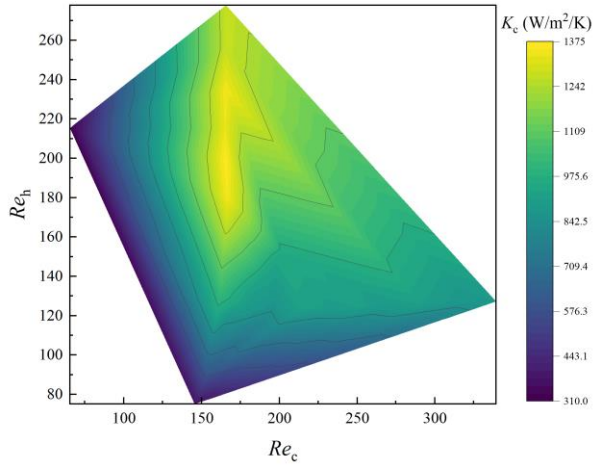

FIGURE 6: VARIATIONS OF OVERALL HEAT TRANSFER COEFFICIENT FOR ALL EXPERIMENTAL DATA.

3.2 Flow characteristics and friction coefficient correlation

In this study, the experimentally measured pressure drop refers to the pressure drop of the water passing through the PCHE, consisting of the core pressure drop, the pressure drop induced by flow acceleration, and the deformation pressure drop caused by expansions and contractions at the headers. To accurately obtain the flow losses within the airfoil-fin channels, following the method employed by Baik et al. [19] and Park et al. [20], this study differentiates and calculates the flow pressure drop of high-pressure water in the core of the cold-side plate through the use of form loss factors.

FIGURE 7 demonstrates the variations of PCHE core pressure drop with *Re* for the cold-side fluid. It indicates that the pressure drop increases with the rise in flow *Re* under the current experimental conditions. This phenomenon contributes to the fact that an increase in *Re* enhances the inertial forces of the water, leading to a significant manifestation of fluid inertia. This, in turn, intensifies flow irregularities, resulting in increased fluid resistance. Near $Re_c = 150$, pressure drop fluctuations occur. This is attributed to the fact that these operating points are under different pressure and inlet temperature conditions, leading to variations in the thermal properties of water compared to other operating points.

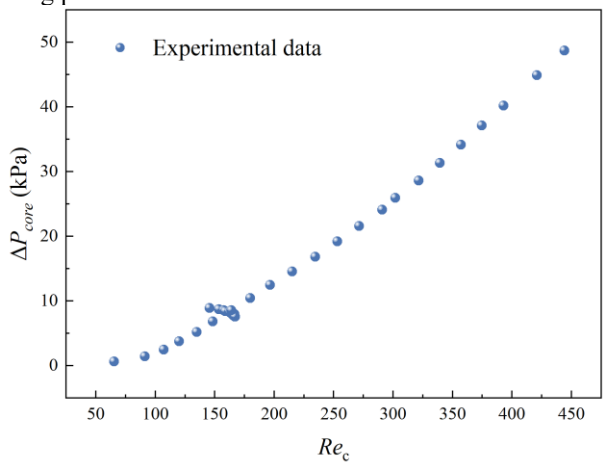

FIGURE 7: PCHE CORE PRESSURE DROP OF COLD-SIDE FLUID.

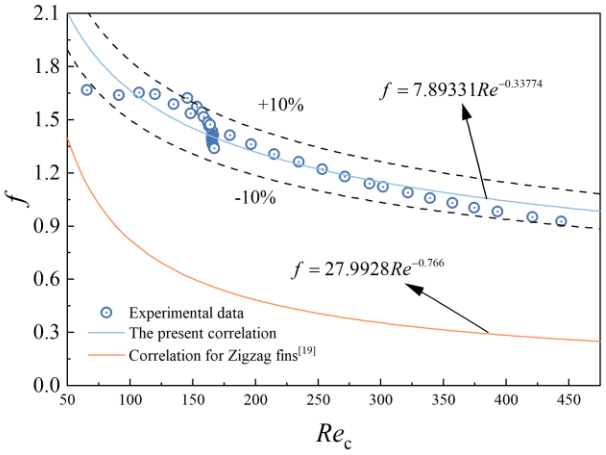

FIGURE 8: VARIATIONS OF FRICTION COEFFICIENT WITH REYNOLDS NUMBER.

Based on the experimental data, a correlation for the friction coefficient of the airfoil-fin channel PCHE has been developed employing nonlinear regression fitting, as shown in Eq. (17). FIGURE 8 illustrates the variations of friction coefficient with *Re* for both experimental results and the present correlation and a comparison with the friction coefficient correlation for zigzag fins [19]. It can be seen that almost all the prediction errors between experimental data and the data predicted by the present correlation are within ±10%, which validates Eq. (17). Furthermore, the correlation for zigzag fins from Ref. [19] is also applicable to water as the working fluid, and the *Re* range studied in the current work is similar to that in Ref. [19]. Therefore, the comparison between the two holds value. It indicates the friction coefficient for the airfoil-fin channels is slightly higher than that for the zigzag-fin channels in the *Re* range of 65.4 to 444.

$$f = 7.89331Re^{-0.33774},\ 65.4 < Re < 444 \quad (17)$$

3.3 Heat transfer characteristics and *Nu* correlation

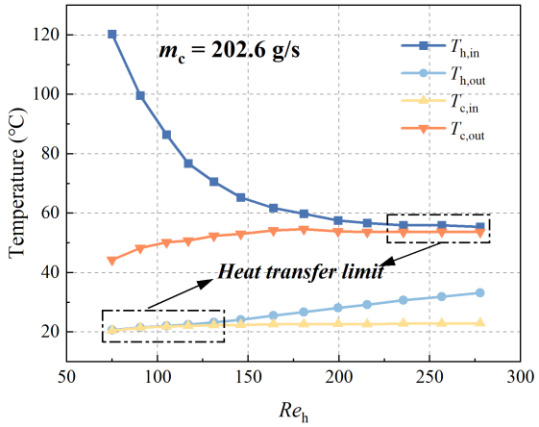

(a) Temperature variations with Re_h

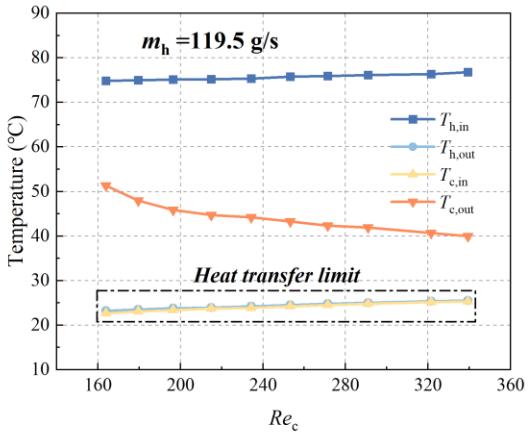

(b) Temperature variations with Re_c

FIGURE 9: PCHE INLET AND OUTLET TEMPERATURES VARIATION WITH REYNOLDS NUMBER.

FIGURE 9 shows the variation of the PCHE inlet and outlet temperatures with the *Re* of the hot/cold-side fluid when the mass flow rate of the other side is kept constant. As depicted in FIGURE 9(a), in the case of m_c = 202.6 g/s, the inlet temperature of the hot-side water ($T_{h,in}$) decreases with the increase in Re_h until it reaches a steady state. This phenomenon is attributed to the gradual reaching of the limits of heat transfer. As Re_h increases, the *K* of the PCHE also increases, enhancing the heat transfer capacity. Consequently, the hot-side water undergoes continuous cooling until it reaches the heat transfer limitation. For the same reasons, the outlet temperature of the cold-side water ($T_{c,out}$) continuously increases until it reaches a steady state. As for the outlet temperature of the hot-side water ($T_{h,out}$), $T_{h,out}$ increases monotonically with Re_h due to the increase in total heat on the hot side with the growth of Re_h. Due to the strong cooling capacity of the water cooler, the inlet temperature of the cold-side water ($T_{c,in}$) remains essentially constant. When m_h is fixed at 119.5 g/s and the *Re* of the cold-side water (Re_c) is continuously increased, the PCHE inlet and outlet temperature variation is plotted in FIGURE 9(b). Since the heat transfer capacity of the PCHE is designed at above 175 kW class and the experimental setup has limited capabilities (with a maximum heat transfer capacity of approximately 40 kW), in most operating conditions, the heat transfer limit is approached, and $T_{h,out}$ approaches $T_{c,in}$. Similar to the analysis discussed above, with Re_c increasing, the *K* of the PCHE increases and the total cooling capacity on the cold side also increases. Therefore, $T_{c,out}$ decreases monotonically with Re_c.

To accurately predict the heat transfer performance of high-pressure water within the airfoil-fin PCHE, fitting the *Nu* correlation based on experimental data is crucial. Considering the structural similarity between the cold and hot-side plates of the PCHE, the identical airfoil fins, and the use of high-pressure water as the working fluid on both sides, it can be assumed that the *Nu* correlations for the cold and hot-side water are entirely identical, following the form of the Dittus-Boelter equation, as shown below:

$$Nu = \alpha Re^{\beta} Pr^{1/3} \tag{18}$$

where α and β are constants to be determined.

By combining Eq. (11), Eq. (12) and Eq. (18) and simplifying, Eq. (19) can be obtained:

$$R = \frac{\Delta T_m}{Q_{ave}} = \frac{d}{\alpha Re_h^{\beta} Pr_h^{1/3} \lambda_h A_h} + \frac{\delta}{A_w \lambda_w} + \frac{d}{\alpha Re_c^{\beta} Pr_c^{1/3} \lambda_c A_c} \tag{19}$$

As we can see, Eq. (19) involves only two unknown constants (α and β). Therefore, based on experimental data, the values of α and β can be uniquely determined using the least squares fitting method. FIGURE 10 illustrates the comparison between the fitted calculated overall thermal resistance of PCHE and the experimental data. The relative deviation of all results falls within ±20%, validating the reliability of the fitting results.

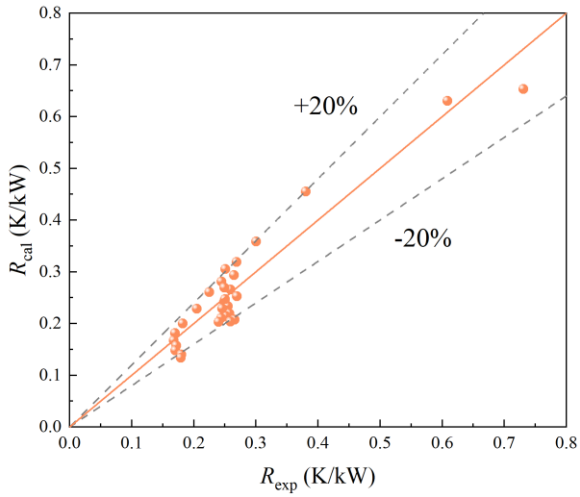

FIGURE 10: COMPARISON OF THE OVERALL THERMAL RESISTANCE.

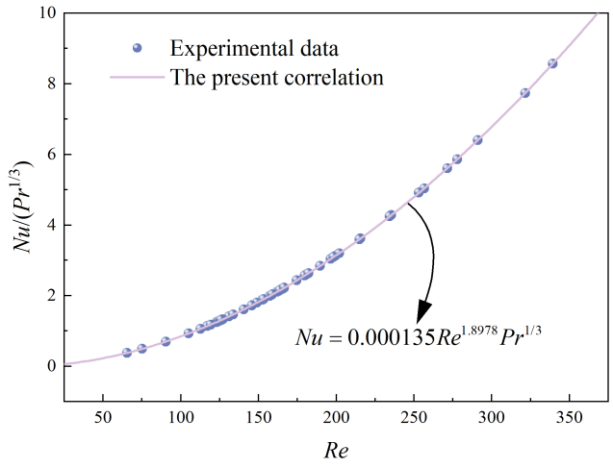

FIGURE 11: NUSSELT NUMBER CORRELATION FOR HIGH-PRESSURE WATER.

Finally, the *Nu* correlation of high-pressure water for the airfoil-fin PCHE is developed, as presented in Eq. (20). FIGURE 11 illustrates the distribution of the proposed correlation and the experimental data points for the *Nu*. It can be observed that *Nu* increases exponentially with the growth of *Re*, and the distribution of experimental data for *Nu* is relatively uniform.

$$Nu = 0.000135Re^{1.8978}Pr^{1/3},\ 50 < Re < 350,\ 2.0 < Pr < 5.1 \quad (20)$$

Based on Eq. (20) and Eq. (12), the HTC of hot-side water and cold-side water for all experimental data can be calculated, as displayed in FIGURE 12. In the experimental data, the maximum HTC is 10434.1 W/m^2/K, occurring at the condition of $Re_c = 339$ and $Re_h = 127$. Even at such extremely low *Re*, water within the airfoil-fin channels still exhibits a high HTC, reaffirming the excellent heat transfer performance of the airfoil-fin PCHE.

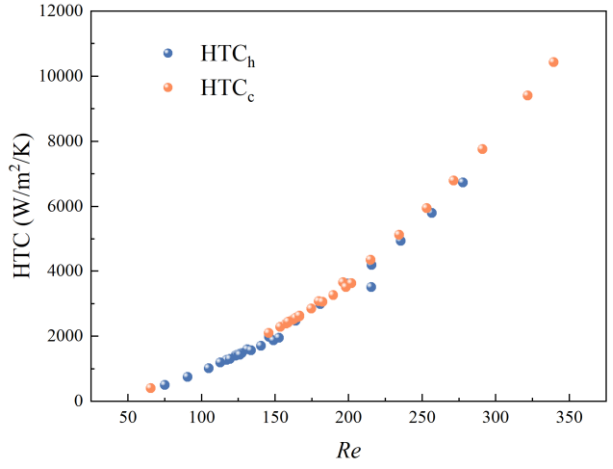

FIGURE 12: HTC VARIATIONS WITH REYNOLDS NUMBER.

4. CONCLUSION

The present study constructs an experimental platform with two high-pressure water loops to experimentally investigate the thermal-hydraulic performance of the airfoil-fin PCHE. The friction coefficient correlation is developed within ±10% deviation with the experimental data. The *Nu* correlation is also proposed, having a maximum deviation of ±20%. The airfoil-fin PCHE exhibits excellent thermal-hydraulic performance, with a friction coefficient slightly higher than that of zigzag fins. Even at extremely low *Re* (Re_h = 199.4 and Re_c = 165.4), K_c can still reach 1370.5 W/m^2/K. In conclusion, the results can contribute to designing and optimizing high-performance PCHE with airfoil fins for advanced thermal management systems.

ACKNOWLEDGEMENTS

This study is supported by the Fundamental Research Funds for the Central Universities (No. 501XTCX2023146001) and the National Science and Technology Major Project of China (No. J2019-III-0015-0059).

REFERENCES

[1] Chai L, Tassou SA. A review of printed circuit heat exchangers for helium and supercritical CO2 Brayton cycles. Thermal Science and Engineering Progress. 2020;18:22.
[2] Saeed M, Kim M-H. Thermal-hydraulic analysis of sinusoidal fin-based printed circuit heat exchangers for supercritical CO2 Brayton cycle. Energy Conversion and Management. 2019;193:124-39.
[3] Kim IH, No HC. Physical model development and optimal design of PCHE for intermediate heat exchangers in HTGRs. Nuclear Engineering and Design. 2012;243:243-50.
[4] Yoon SH, No HC, Kang GB. Assessment of straight, zigzag, S-shape, and airfoil PCHEs for intermediate heat exchangers of HTGRs and SFRs. Nuclear Engineering and Design. 2014;270:334-43.
[5] Zhang H, Shi L, Xuan W, Chen T, Li Y, Tian H, et al. Analysis of printed circuit heat exchanger (PCHE) potential in exhaust waste heat recovery. Applied Thermal Engineering. 2022;204.
[6] Chang H, Lian J, Ma T, Li L, Wang Q. Design and optimization of an annular air-hydrogen precooler for advanced space launchers engines. Energy Conversion and Management. 2021;241.
[7] Fu Y, Liu W, Qi H, Chen Q, Wen J, Xu G. Heat transfer area optimization of intermediate heat-exchange cycle system for aero engines. International Journal of Heat and Mass Transfer. 2024;220.
[8] Huang C, Cai W, Wang Y, Liu Y, Li Q, Li B. Review on the characteristics of flow and heat transfer in printed circuit heat exchangers. Applied Thermal Engineering. 2019;153:190-205.
[9] Tang L, Cao Z, Pan J. Investigation on the thermal-hydraulic performance in a PCHE with airfoil fins for supercritical LNG near the pseudo-critical temperature under the rolling condition. Applied Thermal Engineering. 2020;175.
[10] Wang W-Q, Qiu Y, He Y-L, Shi H-Y. Experimental study on the heat transfer performance of a molten-salt printed circuit heat exchanger with airfoil fins for concentrating solar power. International Journal of Heat and Mass Transfer. 2019;135:837-46.
[11] Shi H-Y, Li M-J, Wang W-Q, Qiu Y, Tao W-Q. Heat transfer and friction of molten salt and supercritical CO2 flowing in an

airfoil channel of a printed circuit heat exchanger. International Journal of Heat and Mass Transfer. 2020;150.
[12] Han Z, Guo J, Zhang H, Chen J, Huai X, Cui X. Experimental and numerical studies on novel airfoil fins heat exchanger in flue gas heat recovery system. Applied Thermal Engineering. 2021;192.
[13] Nourafkan E, Karimi G, Moradgholi J. Experimental Study of Laminar Convective Heat Transfer and Pressure Drop of Cuprous Oxide/Water Nanofluid Inside a Circular Tube. Experimental Heat Transfer. 2014;28:58-68.
[14] Chang H, Han Z, Li X, Ma T, Wang Q. Experimental investigation on heat transfer performance based on average thermal-resistance ratio for supercritical carbon dioxide in asymmetric airfoil-fin printed circuit heat exchanger. Energy. 2022;254.
[15] Chung S, Lee SW, Kim N, Shin SM, Kim MH, Jo H. Experimental study of printed-circuit heat exchangers with airfoil and straight channels for optimized recuperators in nitrogen Brayton cycle. Applied Thermal Engineering. 2023;218.
[16] Kim TH, Kwon JG, Yoon SH, Park HS, Kim MH, Cha JE. Numerical analysis of air-foil shaped fin performance in printed circuit heat exchanger in a supercritical carbon dioxide power cycle. Nuclear Engineering and Design. 2015;288:110-8.
[17] Bell IH, Wronski J, Quoilin S, Lemort V. Pure and Pseudo-pure Fluid Thermophysical Property Evaluation and the Open-Source Thermophysical Property Library CoolProp. Ind Eng Chem Res. 2014;53:2498-508.
[18] Taylor J. Introduction to error analysis, the study of uncertainties in physical measurements1997.
[19] Baik S, Kim SG, Lee J, Lee JI. Study on CO2 – water printed circuit heat exchanger performance operating under various CO_2 phases for S-CO_2 power cycle application. Applied Thermal Engineering. 2017;113:1536-46.
[20] Park JH, Kwon JG, Kim TH, Kim MH, Cha J-E, Jo H. Experimental study of a straight channel printed circuit heat exchanger on supercritical CO2 near the critical point with water cooling. International Journal of Heat and Mass Transfer. 2020;150.